SCIENTIFIC REPORTS

OPEN

CONFERENCE PROCEEDINGS

APEnergy2014

SUBJECT AREAS:
BATTERIES
SYNTHESIS AND PROCESSING
NANOPARTICLES

Received
11 February 2014

Accepted
28 March 2014

Published
29 August 2014

Correspondence and requests for materials should be addressed to Y.C.K. (yckang@konkuk.ac.kr)

Rapid continuous synthesis of spherical reduced graphene ball-nickel oxide composite for lithium ion batteries

Seung Ho Choi, You Na Ko, Jung-Kul Lee & Yun Chan Kang

Department of Chemical Engineering, Konkuk University, 1 Hwayang-dong, Gwangjin-gu, Seoul 143-701, Korea.

In this study, we synthesized a powder consisting of core-shell-structured Ni/NiO nanocluster-decorated graphene (Ni/NiO-graphene) by a simple process for use as an anodic material for lithium-ion batteries. First, a crumpled graphene powder consisting of uniformly distributed Ni nanoclusters was prepared by one-pot spray pyrolysis. This powder was subsequently transformed into the Ni/NiO-graphene composite by annealing at 300°C in air. The Ni/NiO-graphene composite powder exhibited better electrochemical properties than those of the hollow-structured NiO-Ni composite and pure NiO powders. The initial discharge and charge capacities of the Ni/NiO-graphene composite powder were 1156 and 845 mA h g^{-1}, respectively, and the corresponding initial coulombic efficiency was 73%. The discharge capacities of the Ni/NiO-graphene, NiO-Ni, and pure NiO powders after 300 cycles were 863, 647, and 439 mA h g^{-1}, respectively. The high stability of the Ni/NiO-graphene composite powder, attributable to the unique structure of its particles, resulted in it exhibiting long-term cycling stability even at a current density of 1500 mA g^{-1}, as well as good rate performance. The structural stability of the Ni/NiO-graphene composite powder particles during cycling lowered the charge transfer resistance and improved the Li-ion diffusion rate.

Ever since transition metal oxides were first found to be suitable as anodic materials for lithium-ion batteries (LIBs), a number of metal oxides with different structures have been studied extensively[1–17]. Generally, metal oxides that exhibit high theoretical capacities have poor Li^+ storage/release properties, owing to the large changes that occur in their volume during cycling and because of their low electrochemical conductivities[1–17]. Of the various transition metal oxides being investigated, NiO has attracted particular attention as a promising anodic material for LIBs, as it is abundantly available, and exhibits low toxicity, high volumetric energy density, and superior safety[18–31]. However, NiO also exhibits poor rate performance and cyclability owing to slow kinetics of its conversion reaction and its low electronic conductivity[18–31]. NiO-Ni composite materials have been studied in order to improve upon the electrochemical properties of NiO[18–20]. Composites comprising ultrafine Ni nanoclusters embedded in an active NiO matrix exhibit high initial Coulombic efficiency, facilitating the decomposition of Li_2O and the solid-electrolyte interface (SEI) film formed during the charge/discharge process[18–20]. In addition, Ni can improve the electrochemical properties of NiO as NiO-Ni composite materials exhibit high electronic conductivities. Consequently, Ni when used as an additive results in NiO-Ni composite materials that exhibit high reversible discharge capacities, initial Coulombic efficiencies, cycling stabilities, and rate capabilities as anodic materials in LIBs[18–20]. In recent years, graphene-based metal oxide composites have also been studied widely for use as high-capacity anodic materials for LIBs[33–37]. Graphene, owing to its excellent mechanical, thermal, and electrical properties, can be used to improve the electrochemical conductivities of metal oxides and can be exploited as a buffer layer in anodic materials. Thus, NiO-graphene composite materials, which exhibit high capacities, have also been investigated for use as anodic materials for LIBs[26–32]. However, to the best of our knowledge, NiO-graphene composite materials that show long-term stability and high rate performances have not yet been reported.

In this study, we fabricated a powder consisting of graphene decorated with core-shell-structured Ni/NiO nanoclusters (Ni/NiO-graphene) by a simple process for use as anodic materials for LIBs. The detailed formation mechanism of the novel-structured Ni/NiO-graphene composite powder was also investigated. First, a powder of crumpled graphene uniformly covered with Ni nanoclusters was prepared by one-pot spray pyrolysis in a nitrogen atmosphere. Then, this Ni-graphene composite was transformed into the NiO/Ni-graphene composite through annealing at 300°C in air. The electrochemical properties of the NiO/Ni-graphene composite powder

were compared with those of a hollow-structured NiO-Ni composite as well as with those of a pure NiO powder prepared by the same process in the absence of graphene. It was found that Ni metal as well as graphene improved the electrochemical properties of NiO.

Results

The formation mechanism of the powder consisting of graphene decorated with core-shell-structured Ni/NiO nanoclusters (i.e., the Ni/NiO-graphene powder) is described in Figure 1. First, a Ni nitrate-graphene oxide composite powder was produced by drying droplets of a nickel nitrate solution containing graphene oxide sheets in a nitrogen atmosphere. The decomposition of nickel nitrate into nickel oxide was also performed in a nitrogen atmosphere, and the reducing atmosphere, attributable to the graphene sheets, reduced the nickel oxide nanoclusters into nanoclusters of Ni metal. Graphene was formed by the thermal reduction of the graphene oxide sheets at the high temperature of 800°C. The graphene oxide/graphene sheets prevented the growth of the NiO/Ni nanoclusters within the composite powder. The graphene powder with spherical particles and a uniform distribution of Ni nanoclusters could be prepared by one-pot spray pyrolysis even when the reaction time was as small as 10 s. The Ni-graphene composite powder was then annealed at the low temperature of 300°C in air, resulting in the partial oxidation of the Ni nanoclusters. This also prevented the decomposition of the graphene. The oxidation of the outer part of the Ni nanoclusters resulted in the formation of the Ni-NiO core-shell nanoclusters. Consequently, the annealing of the Ni-graphene composite powder resulted in the fabrication of the core-shell-structured Ni/NiO nanocluster-decorated graphene (Ni/NiO-graphene) powder.

The hollow-structured NiO-Ni composite powder was prepared by the one-pot spray pyrolysis of a solution of nickel nitrate and sucrose. The decomposition of the sucrose and nickel nitrate in a nitrogen atmosphere produced a hollow-structured NiO-carbon composite as an intermediate product in the front part of the reactor. Simultaneously, sucrose was oxidized by the nitrate anions, resulting in carbon dioxide, nitrogen, and nitrogen dioxide, as well as water, in large amounts[38]. The abrupt evolution of these gases owing to the decomposition of sucrose and nickel nitrate was what produced the hollow-structured powder particles. The reduction of NiO into Ni owing to the consumption of carbon occurred at the rear of the reactor. The fact that the carbonization of sucrose produced carbon in an insufficient amount is what resulted in the hollow-structured carbon-free NiO-Ni composite powder. Finally, a hollow-structured NiO powder was prepared by the spray pyrolysis of a solution of nickel nitrate that did not contain either graphene oxide or sucrose. The thermal decomposition of this nickel nitrate solution in a nitrogen atmosphere resulted in the fabrication of a powder consisting of hollow-structured NiO particles with thick shells.

The XRD patterns of the powders prepared from the various types of spray solutions, obtained before and after annealing in air, are shown in Figure S1. The particles of the powders prepared by the one-pot spray pyrolysis of solutions containing graphene oxide and sucrose primarily had crystal structures similar to those of Ni and NiO, respectively, while the particles of the powder prepared using the spray solution that did not contain a carbon source had a pure-NiO-like crystal structure. In the case of the Ni-graphene composite powder, the oxidation of a large amount of Ni into NiO occurred after annealing at 300°C in air, resulting in the formation of the Ni/NiO-graphene composite powder, as shown in Figure S1b. On the other hand, the hollow-structured NiO-Ni composite powder did not undergo oxidation because of the dense structure of its particles, which were impermeable to the gases produced during the process. The Ni nanoclusters embedded in the NiO matrix were stable at the low annealing temperature of 300°C. Therefore, the hollow-structured NiO-Ni powder particles exhibited the same crystal structure before and after the annealing treatment. The XRD pattern of the NiO powder prepared from the spray solution of nickel nitrate that did not contain graphene oxide or sucrose was similar to that of pure NiO. Figure S2 shows the XPS spectrum for the Ni/NiO-graphene composite powders. The peak at 854.2 eV binding energy was very close to those for the corresponding peaks in the Ni $2p_{3/2}$ spectrum for pure NiO[39,40]. The XPS spectrum did not show a shoulder peak at 852.9 eV, attributable to metallic Ni. Therefore, Ni metal did not exist on the surface of the Ni/NiO nanocrystals dispersed all over the graphene[40]. However, the XRD pattern, as shown in Figure S1, indicated that the Ni/NiO-graphene composite powders contained Ni and NiO mixed crystal structures. Taken together, the XPS and XRD spectra demonstrated that the Ni/NiO nanocrystal core-shell structure was dispersed all over the graphene.

Figure 2 shows the morphology of the Ni/NiO-graphene composite powder prepared by the two-step process. The SEM and low-resolution TEM images shown in Figures 2a–2c suggest that the composite powder particles had a crumpled structure. Ni/NiO nanoclusters several nanometers in size were uniformly distributed all over the graphene powder particles, as shown in the TEM and dot-mapping images. In addition, Ni and carbon were also uniformly distributed all over the particles of the composite powder, as can be seen from the dot-mapping images. Figure S3 shows the thermogravimetric (TG) curves of the powder. The total decrease in the weight of the Ni/NiO-graphene composite powder at 700°C was 4 wt%. The decrease in its weight owing to the decomposition of graphene was reduced because of the weight increase resulting from the oxidation of Ni into NiO. Therefore, the graphene content of the composite powders was higher than 4 wt%. The EDX spectrum of the Ni/NiO-graphene composite powders as shown in Figure S4a shows the clear peak of carbon. The two peaks in the Raman spectrum of the Ni/NiO-graphene composite powder (see Figure S5), observed at 1350 and 1590 cm^{-1}, correspond to the D and G bands of graphene, respectively. Graphene was formed by the thermal reduction of graphene oxide during the preparation of the Ni/NiO-graphene composite powder via spray pyrolysis.

Figure 3 shows the morphology of the hollow-structured NiO-Ni composite powder prepared from the spray solution containing

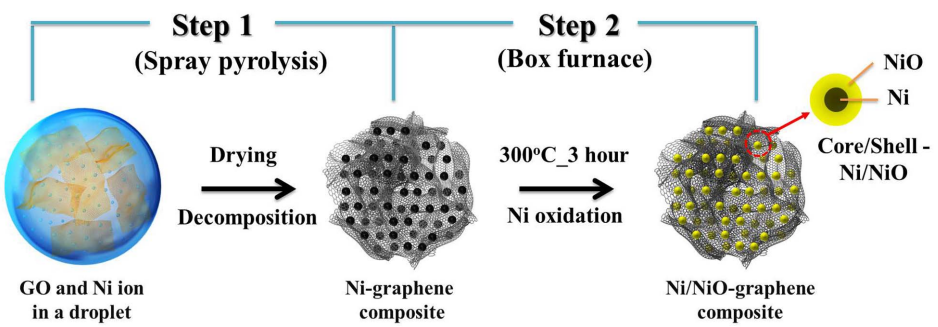

Figure 1 | Formation mechanism of core-shell structured Ni/NiO nanocluster-decorated graphene (Ni/NiO-graphene) composite powder.

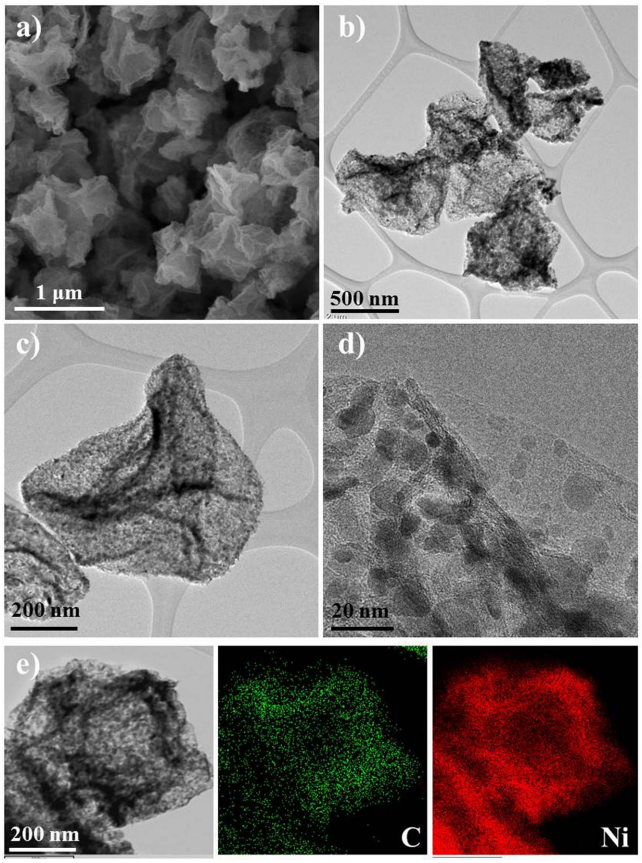

Figure 2 | Morphologies and dot-mapping images of the Ni/NiO-graphene composite powders prepared by two-step process: (a) SEM, (b)–(d) TEM, and (e) dot-mapping images.

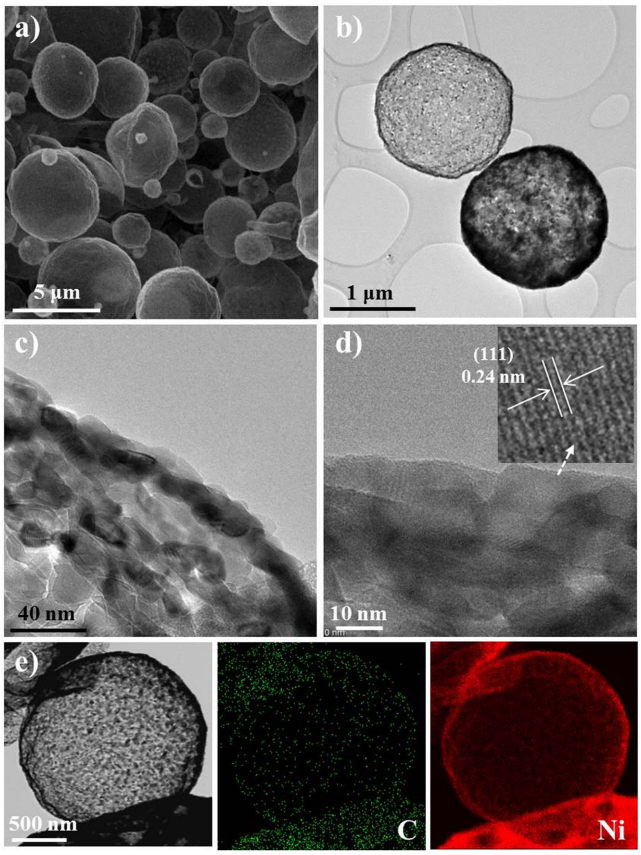

Figure 3 | Morphologies and dot-mapping images of the hollow structured NiO-Ni composite powders: (a) SEM, (b)–(d) TEM, and (e) dot-mapping images.

nickel nitrate and sucrose. The SEM and TEM images show the powder particles had a hollow structure and thin walls. The high-resolution TEM images shown in Figures 3c and 3d reveal that the nanocrystals, which were several tens of nanometers in size, did not form large aggregates. The high-resolution TEM image inset in Figure 3d reveals that the clear lattice fringes of the powder were separated by 0.24 nm; this value corresponds to the (111) crystal plane of NiO[22]. The carbon component was could barely be detected in the dot-mapping images shown in Figure 3e. Figure S4b shows the EDX spectrum of the NiO-Ni composite powder that is shown in Figure 3e; in this case too, the carbon component originating from the carbon grid was not observed. No carbon-related peaks were observed in the spectrum. The weight increase of the NiO-Ni composite powder owing to the oxidation of Ni into NiO was 3.2 wt%, as determined from the TG curve shown in Figure S3. The Ni/NiO weight ratio of the NiO-Ni composite powder as calculated from the TG data was 12/88. Figure S6 shows the morphology of the pure NiO powder prepared directly by the spray pyrolysis of a solution of nickel nitrate that did not contain a carbon source. The SEM image shows that the particles of the NiO powder had a hollow structure. The mean sizes of the particles of the NiO-Ni and NiO powders shown in Figure 3 and Figure S6 were 2.2 and 1.3 μm, respectively. The gases that evolved during the decomposition of sucrose increased the mean size and degree of hollowness of the NiO-Ni powder particles.

The electrochemical properties of the three powder samples are shown in Figure 4. Figure 4a shows the cyclic voltammograms (CVs) of the Ni/NiO-graphene composite powder for the first three cycles at a scan rate of 0.1 mV s^{-1} for voltages of 0.001–3 V. A single primary anodic peak was observed at approximately 0.53 V; this corresponded to the initial reduction of NiO to metallic Ni and the formation of amorphous Li_2O and a solid-electrolyte interface (SEI) layer[26–29]. In addition, two broad oxidation peaks were observed, at 1.5 and 2.3 V, respectively, during the first charging process; these corresponded to the oxidation of the Ni nanograins to NiO and the subsequent decomposition of the SEI layer[26–29]. The main reduction peak shifted to approximately 1.2 V after the first cycle. From the second cycle onward, the reduction and oxidation peaks exhibited substantial overlap. Figure 4b shows the first and second charge/discharge curves of the Ni/NiO-graphene and NiO-Ni composite powders. The operating cut-off voltages were 0.001 and 3 V, respectively, at a constant current density of 1500 mA g^{-1}. The potential of the NiO-Ni composite powder decreased sharply to 0.5 V and then remained constant over the rest of the initial discharge curve. However, the potential of the Ni/NiO-graphene composite powder decreased gradually to 0.53 V during the initial discharging process. The fact that Li could be inserted readily into the particles of the Ni/NiO-graphene composite powder at high voltages was due to the fact that ultrafine NiO/Ni nanoclusters were dispersed in the graphene matrix, resulting in high electrical conductivity. During the first discharge and charge processes, the NiO particles transformed into amorphous NiO nanocrystals, irrespective of their original structure. Therefore, the second discharge curves of the Ni/NiO-graphene and NiO-Ni composite powders had similar shapes, unlike those corresponding to the first discharge cycle. In the second cycle, the wide potential plateau, which can be seen in the first discharge curve, was replaced by a sloping curve that extended from 1.7 V to 0.8 V. The initial discharge and charge capacities of the Ni/NiO-graphene composite powder were 1156 and 845 mA h g^{-1}, respectively, and the corresponding initial Coulombic efficiency was 73%. The initial discharge and charge capacities of the NiO-Ni composite powder were 1009 and 759 mA h g^{-1}, respectively, and the corresponding initial

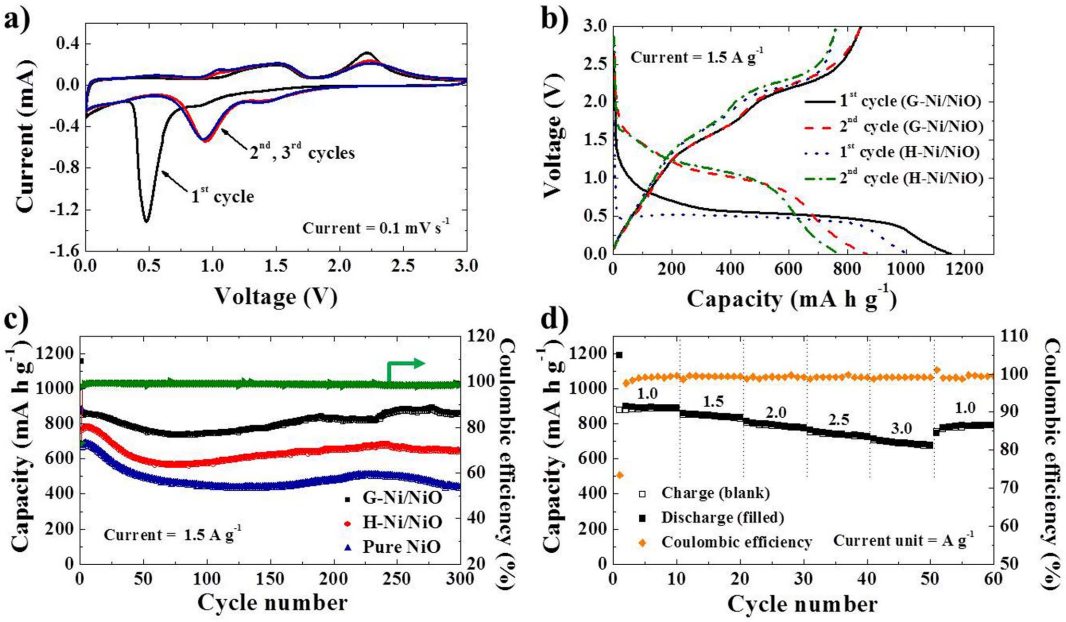

Figure 4 | Electrochemical properties of the three type samples: (a) cyclic voltammograms of the Ni/NiO-graphene, (b) first and second charge/discharge curves of the Ni/NiO-graphene and NiO-Ni, (c) cycling performances at a current density of 1500 mA g^{-1}, and (d) rate performance and Coulombic efficiencies of the Ni/NiO-graphene composite powders.

Coulombic efficiency was 75%. The Ni/NiO-graphene composite powders showed slightly lower initial Coulombic efficiency than the NiO-Ni composite powders because of the graphene component, which showed low initial Coulombic efficiency. However, the low-graphene-content Ni/NiO-graphene composite powders showed higher initial Coulombic efficiencies than those previously reported for NiO-graphene composite powders[26–32].

Figure 4c shows the cycling performances of the three powders at a current density of 1500 mA g^{-1}. The discharge capacities of the NiO-Ni composite powder, which had a high Ni/NiO weight ratio, increased for the first 5 cycles, and then decreased sharply for the next 70 cycles. This decrease in the discharge capacity was inevitable, given the microscale structural damage that is incurred by NiO powders at high current densities, starting at the first cycle. Therefore, the increase in the discharge capacities of the NiO-Ni composite powder was due to the gradual activation of the Ni metal during the first 5 cycles as shown in Figure S7. The step-by-step activation of Ni retarded the decrease in the discharge capacity of the Ni/NiO-graphene composite powder for the first several cycles. The discharge capacity of the pure NiO powder also increased slightly for the first 4 cycles. In the case of the pure NiO powder, the incomplete lithiation of the thick NiO layer at a high current density of 1500 mA g^{-1} during the first discharge process increased the discharge capacity during the first 4 cycles. However, an increase in the discharge capacity was not observed in the case of the Ni/NiO-graphene composite powder, owing to its low Ni content. The decrease in the discharge capacity of the Ni/NiO-graphene composite powder was lower than those in the cases of the NiO-Ni composite and pure NiO powders during the first 70 cycles. This was because of the structural stability of the Ni/NiO-graphene composite powder. The graphene layers reduced the change in the volume of the core-shell structured Ni/NiO nanoclusters and prevented the growth of Ni crystals during cycling. The discharge capacities of the Ni/NiO-graphene, NiO-Ni, and pure NiO powders after 300 cycles were 863, 647, and 439 mA h g^{-1}, respectively. The Coulombic efficiency of the Ni/NiO-graphene composite powder is also shown in Figure 4c. The Coulombic efficiency of the Ni/NiO-graphene composite powder stayed high, at greater than 99%, after the 3th cycle. Figure S8 shows SEM images of the Ni/NiO-graphene and NiO-Ni composite powders after they had been subjected to 300 charge/discharge cycles at a current density of 1500 mA g^{-1}. The overall structure of the Ni/NiO-graphene composite powder particles remained unchanged even after 300 cycles. On the other hand, the spherical particles of the NiO-Ni composite powder, which had smooth surfaces, transformed into particles with a crumpled structure after cycling. Owing to its high structural stability, the Ni/NiO-graphene composite powder exhibited long-term stability even at a current density of 1500 mA g^{-1}. The highly dispersed Ni nanoclusters in the Ni/NiO-graphene composite resulted in the more complete decomposition of the Li_2O formed during the discharging process. The decomposition process can be represented by the following reaction: $Ni + Li_2O \rightarrow NiO + 2Li^+ + 2e^-$)[18–20]. The Ni nanoclusters in the Ni/NiO-graphene composite powder acted as highly conductive pathways for electron transfer during the conversion reaction of NiO with Li^+[18–20].

Figure 4d shows the rate performance of the Ni/NiO-graphene composite powder. The current density was increased from 1000 mA g^{-1} to 3000 mA g^{-1} in a stepwise manner, and then decreased to 1000 mA g^{-1}. The Ni/NiO-graphene composite powder exhibited a second discharge capacity of 899 mA h g^{-1} at a current density of 1000 mA g^{-1}. Even at a high current density of 3000 mA g^{-1}, the discharge capacity of the Ni/NiO-graphene composite powder was as high as 700 mA h g^{-1} after 40 cycles, when the current density was increased in a stepwise manner. The discharge capacity decreased with an increase in the number of cycles for current densities of 1500–3000 mA g^{-1}; this was owing to the structural damage incurred by the powder particles, as described previously (see Figure 4c). Therefore, the Ni/NiO-graphene composite powder had a better rate performance than that shown in Figure 4d. Finally, the Ni/NiO-graphene composite powder exhibited Coulombic efficiencies greater than 99% even at high current densities.

Discussion

Electrochemical impedance spectroscopy was performed to elucidate the Li^+ ion transfer behaviors of the Ni/NiO-graphene and NiO-Ni composite powders. The Nyquist impedance plots of the powders, obtained before cycling and after 100 cycles, are shown in Figure 5. In

the case of the Ni/NiO-graphene composite powder, the diameter of the semicircular curve, which is indicative of the charge-transfer resistance (R_{ct}) and was obtained before cycling for medium-range frequencies, was greater than that in the case of the NiO-Ni composite powder, as can be seen from Figure 5a. The R_{ct} value of the Ni/NiO-graphene composite powder, which had a high Brunauer-Emmett-Teller (BET) surface area, was larger than that of the NiO-Ni composite powder before cycling. The BET surface areas of the Ni/NiO-graphene and NiO-Ni composite powders were 40.7 and 10.6 $m^2\ g^{-1}$, respectively. The R_{ct} value of the Ni/NiO-graphene composite powder decreased after cycling because its particles became amorphous after 100 cycles. On the other hand, the R_{ct} value of the NiO-Ni composite powder increased after 100 cycles. The decrease in the R_{ct} value owing to the formation of particles with an amorphous structure was diminished by the increase resulting from the change in particle structure during cycling[41,42]. Figures 5c and 5d show the relationship between the real part of the impedance (Z_{re}) and $\omega^{-1/2}$ (where ω is the angular frequency, $\omega = 2\pi f$) in the low-frequency region before cycling and after 100 cycles[42–44]. That the slope, σ, which is the Warburg impedance coefficient of the Z_{re} versus $\omega^{-1/2}$ curve, was low indicates that the Li-ion diffusion rate of the Ni/NiO-graphene composite powder was high[40–42]. The structural stability of the Ni/NiO-graphene composite powder during cycling lowered the charge-transfer resistance and improved the Li-ion diffusion rate. The electrochemical properties of the Ni/NiO-graphene composite powders prepared using spray pyrolysis were compared to those of the NiO-graphene composite materials previously reported in the literature, and the results are summarized in Table S1. The Ni/NiO-graphene composite powders showed higher initial discharge capacities and better cycling performances than the previously reported NiO-graphene composite materials. The highly conductive Ni metal and graphene were responsible for the superior electrochemical properties of the Ni/NiO-graphene composite powders.

In summary, a powder consisting of crumpled graphene covered with uniformly distributed core-shell-structured Ni/NiO nanoclusters was prepared by spray pyrolysis. The electrochemical properties of the Ni/NiO-graphene composite powder were compared with those of NiO-Ni composite and pure NiO powders prepared by the same process. The Ni/NiO-graphene composite powder exhibited higher initial discharge and charge capacities and better cycling performance than those of the NiO-Ni composite and pure NiO powders. In addition, the NiO-Ni composite powder showed better electrochemical properties than those of the pure NiO powder, even though the two had similar morphologies. The Ni metal and graphene of the Ni/NiO-graphene composite were responsible for its superior electrochemical properties. The graphene layers retarded the destroy of the core-shell-structured Ni/NiO nanoclusters by large volume change and prevented Ni crystal growth during cycling.

Methods

Material fabrication. *Synthesis of the solution for spray pyrolysis production of Ni/NiO-graphene composite.* Graphene oxide (GO) was synthesized from graphite flakes by a modified Hummers method[12]. Concentrated H_2SO_4 (120 mL) was added to the graphite flakes (4 g) and cooled to 0°C using an ice bath. $KMnO_4$ (12 g) was added stepwise to keep the reaction temperature below 10°C. After removing the solution from the ice bath, it was warmed to 35°C and stirred for 30 min, and then distilled water (120 mL) was slowly added. External heating was introduced to maintain the reaction temperature at 80°C for 20 min. Then, the solution was cooled and additional 500 mL of distilled water (5 wt% H_2O_2) was added. The black precipitate (graphite oxide) was thoroughly washed to remove completely the residual salts and acids and then centrifuged at 4,000 rpm. The as-obtained graphite oxide was re-dispersed in distilled water and then exfoliated to generate graphene oxide sheets by ultrasonication. Nickel nitrate hexahydrate was dissolved into the colloidal solution of graphite oxide.

Synthesis of Ni/NiO-graphene composite. The Ni-graphene composite powders were directly prepared by spray pyrolysis. A schematic diagram of the ultrasonic spray pyrolysis system is shown in Figure S9. A quartz reactor of 1200 mm length and 50 mm diameter was used, and its temperature was maintained at 800°C. The flow rate of nitrogen used as carrier gas was 5 $L{\cdot}min^{-1}$. As-prepared Ni-graphene com-

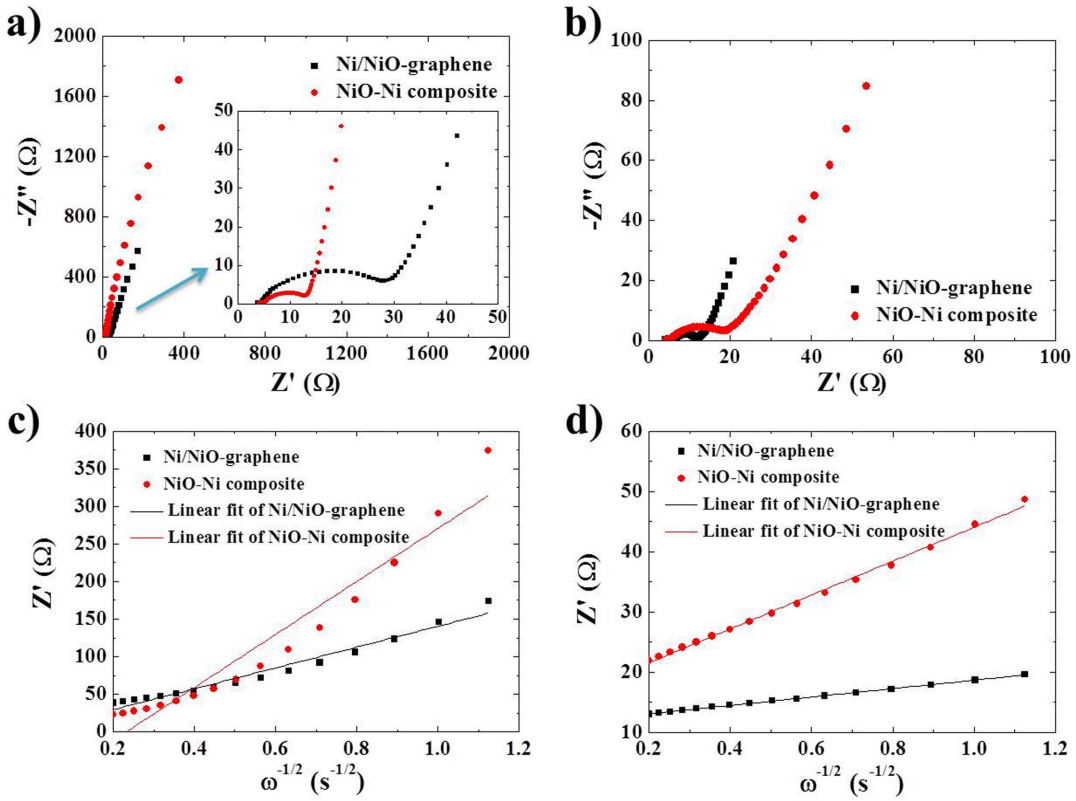

Figure 5 | Nyquist impedance plots and relationships between real part of the impedance (Z_{re}) and $\omega^{-1/2}$ obtained before cycling and after 100 cycles: (a) and (c) before cycling, (b) and (d) after cycling.

posite powders were post-treated at 300°C under an air atmosphere to form the Ni/NiO-graphene composite powders.

Synthesis of NiO-Ni composite and pure NiO powders. The NiO-Ni composite and pure NiO powders were directly prepared by spray pyrolysis from the spray solutions with and without sucrose, respectively, at the same preparation conditions for the Ni-graphene composite powders.

Characterization. The crystal structures of the powders were investigated by X-ray diffractometry (XRD, X'pert PRO MPD) using Cu Kα radiation (λ = 1.5418 Å). Morphological features were investigated using field-emission scanning electron microscopy (FE-SEM, Hitachi S-4800, KBSI Suncheon center) and high-resolution transmission electron microscopy (HR-TEM, JEM-2100F) operating at a working voltage of 200 kV. The specific surface areas of the Ni/NiO-graphene and NiO-Ni composite powders were calculated from Brunauer–Emmett–Teller (BET) analysis of nitrogen adsorption measurements (TriStar 3000). The XPS spectra of the powders were investigated using X-ray photoelectron spectroscopy (XPS, ESCALAB-210) with Al Ka radiation (1486.6 eV).

Electrochemical measurements. The capacities and cycling properties of the powders were determined using a 2032-type coin cell. The electrode was prepared from a mixture containing 70 wt% active material, 20 wt% Super P, and 10 wt% sodium carboxymethyl cellulose (CMC) binder. Lithium metal and microporous polypropylene film were used as the counter electrode and separator, respectively. The electrolyte was a solution of 1 M $LiPF_6$ in a 1 : 1 volume mixture of ethylene carbonate/dimethyl carbonate (EC/DMC) containing 2% vinylene carbonate. The charge/discharge characteristics of the samples were determined through cycling in the 0.001–3 V potential range at a set of fixed current densities. Cyclic voltammetry (CV) measurements were carried out at a scan rate of 0.1 $mV \cdot s^{-1}$. Electrochemical impedance spectroscopy (EIS) was measured using an electrochemical impedance spectroscopy (EIS) over a frequency range of 0.01 Hz – 100 kHz.

1. Poizot, P., Laruelle, S., Grugeon, S., Dupont, L. & Tarascon, J. M. Nano-sized transition-metal oxides as negative-electrode materials for lithium-ion batteries. *Nature* **407**, 496–499 (2000).
2. Bruce, P. G., Scrosati, B. & Tarascon, J. M. Nanomaterials for rechargeable lithium batteries. *Angew. Chem. Int. Ed.* **47**, 2930–2946 (2008).
3. Reddy, M. V., Rao, G. V. S. & Chowdari, B. V. R. Metal oxides and oxysalts as anode materials for Li ion batteries. *Chem. Rev.* **10**, 5364–5457 (2013).
4. Wang, Z., Zhou, L. & Lou, X. W. Metal oxide hollow nanostructures for lithium-ion batteries. *Adv. Mater.* **24**, 1903–1911 (2012).
5. Lai, X. Y., Halpert, J. E. & Wang, D. Recent advances in micro-/nano-structured hollow spheres for energy applications: from simple to complex systems. *Energy Environ. Sci.* **5**, 5604–5618 (2012).
6. Choi, N. S. *et al.* Challenges facing lithium batteries and electrical double-layer capacitors. *Angew. Chem. Int. Ed.* **51**, 9994–10024 (2012).
7. Scrosati, B., Hassoun, J. & Sun, Y. K. Lithium-ion batteries. a look into the future. *Energy Environ. Sci.* **4**, 3287–3295 (2011).
8. Zhang, L., Wu, H. B. & Lou, X. W. Iron-oxide-based advanced anode materials for lithium-ion batteries. *Adv. Energy Mater.* **4**, 1300958 (2014).
9. Yang, S. B. *et al.* Porous iron oxide ribbons grown on graphene for high-performance lithium storage. *Sci. Rep.* **2**, 427 (2012).
10. Zeng, L., Zheng, C., Deng, C., Ding, X. & Wei, M. MoO_2-ordered mesoporous carbon nanocomposite as an anode material for lithium-ion batteries. *ACS Appl. Mater. Interfaces* **5**, 2182–2187 (2013).
11. Mao, S. *et al.* A general approach to one-pot fabrication of crumpled graphene-based nanohybrids for energy applications. *ACS Nano* **6**, 7505–7513 (2012).
12. Choi, S. H. & Kang, Y. C. Crumpled graphene–molybdenum oxide composite powders: preparation and application in lithium-ion batteries. *ChemSusChem* **7**, 523–528 (2014).
13. Kim, C. J., Noh, M. J., Choi, M. S., Cho, J. P. & Park, B. W. Critical size of a nano SnO_2 electrode for Li-secondary battery. *Chem. Mater.* **17**, 3297–3301 (2005).
14. Park, M. S. *et al.* Preparation and electrochemical properties of SnO_2 nanowires for application in lithium-ion batteries. *Angew. Chem. Int. Ed.* **46**, 750–753 (2007).
15. Chen, S., Bao, P. & Wang, G. Synthesis of Fe_2O_3–CNT–graphene hybrid materials with an open three-dimensional nanostructure for high capacity lithium storage. *Nano Energy* **2**, 425–434 (2013).
16. Wu, Z. S. *et al.* Graphene anchored with Co_3O_4 nanoparticles as anode of lithium ion batteries with enhanced reversible capacity and cyclic performance. *ACS Nano* **4**, 3187–3194 (2010).
17. Hassan, M. F., Guo, Z. P., Chen, Z. & Liu, H. K. Carbon-coated MoO_3 nanobelts as anode materials for lithium-ion batteries. *J. Power sources* **195**, 2372–2376 (2010).
18. Li, X. F., Dhanabalan, A. & Wang, C. L. Enhanced electrochemical performance of porous NiO–Ni nanocomposite anode for lithium ion batteries. *J. Power sources* **196**, 9625–9630 (2011).
19. Luo, C. H. *et al.* Preparation of C/Ni.NiO composite nanofibers for anode materials in lithium-ion batteries. *Appl. Phys. A* **113**, 683–692 (2013).
20. Wen, W., Wu, J. M. & Cao, M. H. NiO/Ni powders with effective architectures as anode materials in Li-ion batteries. *J. Mater. Chem. A* **1**, 3881–3885 (2013).
21. Su, D., Ford, M. & Wang, G. Mesoporous NiO crystals with dominantly exposed {110} reactive facets for ultrafast lithium storage. *Sci. Rep.* **2**, 924 (2012).
22. Huang, X. H., Tu, J. P., Zhang, C. Q. & Xiang, J. Y. Net-structured NiO–C nanocomposite as Li-intercalation electrode material. *Electrochem. Commun.* **9**, 1180–1184 (2007).
23. Varghese, B. *et al.* Fabrication of NiO nanowall electrodes for high performance lithium ion battery. *Chem. Mater.* **20**, 3360–3367 (2008).
24. Choi, S. H., Lee, J. H. & Kang, Y. C. One-pot rapid synthesis of core–shell structured NiO@TiO_2 nanopowders and their excellent electrochemical properties as anode materials for lithium ion batteries. *Nanoscale* **5**, 12645–12650 (2013).
25. Wei, S. *et al.* Multifunctional composite core–shell nanoparticles. *Nanoscale* **3**, 4474–4502 (2011).
26. Zhou, G. *et al.* Oxygen bridges between NiO nanosheets and graphene for improvement of lithium storage. *ACS Nano* **4**, 3214–3223 (2012).
27. Zou, Y. & Wang, Y. NiO nanosheets grown on graphene nanosheets as superior anode materials for Li-ion batteries. *Nanoscale* **3**, 2615–2620 (2011).
28. Mai, Y. J. *et al.* NiO–graphene hybrid as an anode material for lithium ion batteries. *J. Power Sources* **204**, 155–161 (2012).
29. Kottegoda, I. R. M., Idris, N. H., Lu, L., Wang, J. Z. & Liu, H. K. Synthesis and characterization of graphene–nickel oxide nanostructures for fast charge–discharge application. *Electrochim. Acta* **56**, 5815–5822 (2011).
30. Qiu, D. *et al.* Graphene anchored with mesoporous NiO nanoplates as anode material for lithium-ion batteries. *J. Solid State Electrochem.* **16**, 1889–1892 (2012).
31. Huang, Y. *et al.* Self-assembly of ultrathin porous NiO nanosheets/graphene hierarchical structure for high-capacity and high-rate lithium storage. *J. Mater. Chem.* **22**, 2844–2847 (2012).
32. Xie, D. *et al.* Synthesis of porous NiO-wrapped graphene nanosheets and their improved lithium storage properties. *J. Phys. Chem. C* **117**, 24121–24128 (2013).
33. Gong, Y. *et al.* Graphene-network-backboned architectures for high-performance lithium storage. *Adv. Mater.* **25**, 3979–3984 (2013).
34. Huang, X., Qi, X., Boey, F. & Zhang, H. Graphene-based composites. *Chem. Soc. Rev.* **41**, 666–686 (2012).
35. Luo, J. Y. *et al.* Crumpled graphene-encapsulated Si nanoparticles for lithium ion battery anodes. *J. Phys. Chem. Lett.* **3**, 1824–1829 (2012).
36. Wu, Z. S. *et al.* Graphene/metal oxide composite electrode materials for energy storage. *Nano Energy* **1**, 107–131 (2012).
37. Xin, S., Guo, Y. G. & Wan, L. J. Nanocarbon networks for advanced rechargeable lithium batteries. *Accounts Chem. Res.* **45**, 1759–1769 (2012).
38. Amarilla, J. M., Rojas, R. M. & Rojo, J. M. Understanding the sucrose-assisted combustion method: effects of the atmosphere and fuel amount on the synthesis and electrochemical performances of $LiNi_{0.5}Mn_{1.5}O_4$ spinel. *J. Power Sources* **196**, 5951–5959 (2011).
39. Xia, X. *et al.* Fabrication of metal oxide nanobranches on atomic-layer-deposited TiO_2 nanotube arrays and their application in energy storage. *Nanoscale* **5**, 6040–6047 (2013).
40. Chen, Y. S. *et al.* Microscopic mechanism for unipolar resistive switching behaviour of nickel oxides. *J. Phys. D: Appl. Phys.* **45**, 065303 (2012).
41. Choi, S. H. & Kang, Y. C. Yolk–Shell, hollow, and single-crystalline $ZnCo_2O_4$ Powders: preparation using a simple one-pot process and application in lithium-ion batteries. *ChemSusChem* **6**, 2111–2116 (2013).
42. Takami, N., Satoh, A., Hara, M. & Ohsaki, T. Structural and kinetic characterization of lithium intercalation into carbon anodes for secondary lithium batteries. *J. Electrochem. Soc.* **142**, 371–379 (1995).
43. Shi, Y. *et al.* Hollow structured Li_3VO_4 wrapped with graphene nanosheets in situ prepared by a one-pot template-free method as an anode for lithium-ion batteries. *Nano Lett.* **13**, 4715–4720 (2013).
44. Ko, Y. N., Park, S. B., Jung, K. Y. & Kang, Y. C. One-pot facile synthesis of ant-cave-structured metal oxide−carbon microballs by continuous process for use as anode materials in Li-ion batteries. *Nano Lett.* **15**, 5462–5466 (2013).

Acknowledgments

This work was supported by the National Research Foundation of Korea (NRF) grant funded by the Korea government (MEST) (No. 2012R1A2A2A02046367). This work was supported by the Energy Efficiency & Resources Core Technology Program of the Korea Institute of Energy Technology Evaluation and Planning (KETEP), granted financial resource from the Ministry of Trade, Industry & Energy, Republic of Korea (201320200000420).

Author contributions

S.H.C., Y.N.K., J.K.L. and Y.C.K. devised the concept, designed the experiment, and wrote the manuscript. S.H.C. and Y.N.K. performed the experiments and analyzed the data. Y.C.K. supervised the project. All authors discussed the results and contributed in this manuscript.

Additional information

Supplementary information accompanies this paper at http://www.nature.com/scientificreports

Competing financial interests: The authors declare no competing financial interests.

How to cite this article: Choi, S.H., Ko, Y.N., Lee, J.-K. & Kang, Y.C. Rapid continuous synthesis of spherical reduced graphene ball-nickel oxide composite for lithium ion batteries. *Sci. Rep.* **4**, 5786; DOI:10.1038/srep05786 (2014).